Available online at www.sciencedirect.com
SCIENCE DIRECT
Journal of Hydrology 312 (2005) 256–276
Journal of Hydrology
www.elsevier.com/locate/jhydrol

A numerical modeling study on desert oasis self-supporting mechanisms

Peter C. Chu[a,*], Shihua Lu[b], Yuchun Chen[b]

[a]Naval Ocean-Atmospheric Prediction Laboratory, Department of Oceanography, Naval Postgraduate School, Monterey, CA 93943, USA
[b]Institute of Cold and Arid Environment and Engineering, Chinese Academy of Sciences, Lanzhou, China

Received 1 December 2003; revised 10 January 2005; accepted 11 February 2005

Abstract

Oasis self-supporting mechanisms due to oasis breeze circulation (OBC) are proposed and simulated numerically in this study using a coupled mesoscale and land-surface model. Excessive evaporation from the oasis makes the oasis surface colder than the surrounding desert surface. The sensible heat-flux gradient from oasis to surrounding desert drives the OBC with downdraft over the oasis and updraft over the desert. The horizontal length-scale of the OBC is around four times as large as the oasis scale. This secondary circulation creates two mechanisms to reduce heat and moisture exchange between the oasis and the surrounding desert: (1) the updraft over the desert reduces low-level hot, dry air flowing from the desert into the oasis; and (2) the downdraft increases the atmospheric static stability that reduces the oasis evaporation. Reduction of the oasis scale weakens the oasis self-supporting mechanisms through the decrease of the OBC associated with the increase of the oasis surface evaporation and decrease of the atmospheric stability over the oasis.

Keywords: Oasis self-supporting mechanism; Oasis breeze circulation; Atmospheric static stability; Wet–cold island; Lift index

1. Introduction

Oases in the arid region of northwestern China (NWC) are originally formed from melting snow in Tianshan and Jilienshan Mountains. Although NWC oases represent only a very small portion (5%) of the land-surface, they are important for agricultural and human activities with more than 95% of the population in NWC. In the last half-century, however, the rapid growth of population and the overexploitation of water soil, and biological resources have led to drought, salinization, and desertification and consequently have hindered the development of sustainable agriculture. For example, Lin et al. (2001) identified that groundwater reservoirs with sustainable water supply equivalent to 44.65×10^8 m^3 year^{-1} is needed to possibly implement several projects in the Kashi Plain in the western Terim Basin to keep the oasis

* Corresponding author. Tel.: +1 831 656 3688; fax: +1 831 656 3686.
E-mail addresses: pcchu@nps.edu (P.C. Chu), chu@nps.navy.mil (P.C. Chu).
URL: http://www.oc.nps.navy.mil/~chu.

0022-1694/$ - see front matter © 2005 Elsevier B.V. All rights reserved.
doi:10.1016/j.jhydrol.2005.02.043

ecological and agricultural environment. Planting tree windbreaks may also improve oasis environment (Kurose et al., 2002). Besides the human effect, atmospheric effect may also be important for the oasis maintenance.

Fig. 1 shows NWC oases near Zhangye and surrounding topography. The Landsat image (Fig. 1) indicates that the oasis size is around 15 km. The heterogeneous surface between oasis and surrounding desert may generate local atmospheric circulation. A Sino-Japanese joint investigation of the atmosphere–land-surface interaction experiment at Heihe River Basin (HEIFE) in NWC (Fig. 2) was carried out from 1988 to 1993 to investigate the atmospheric characteristics in oasis and surrounding desert. The HEIFE area is located near the north edge of the Tibetan Plateau and the ground level ranges from 1400 to 2000 m above the sea level. The size of the area is about 70 km×140 km (Fig. 2). Several distinct daytime features are discovered during HEIFE: (1) the oasis is a wet–cold island capped by warm, dry air in the upper layer that would be advected from the surrounding desert (Tsukamoto et al., 1992, 1995); (2) a thermal inversion layer develops over the Zhangye Oasis from the surface to 8 m height with 2 °C difference when the wind speed was strong (Kai et al., 1997); and (3) water vapor flux is downward over the Gobi desert (Wang and Mitsuta, 1992).

As part of HEIFE, the fundamental observational period observations were carried out at the Zhangye Oasis and the desert in the Hexi Corrider of Gansu Province, China (Kai et al., 1997). The Zhangye Oasis extends about 15 km (NW–SE) by 25 km (NE–SW), and is surrounded by sandy and Gobi deserts. Small sensible heat-flux and dominating latent heat-flux in the surface energy balance during the day (Kai et al., 1997) cause the oasis to be cool and wet. Observation (Hu et al., 1994) shows that the desert surface is drier than the oasis surface all day long. The oasis surface is colder than the desert surface during the day.

The thermal heterogeneity of land-surface can produce local circulations as strong as sea breezes (e.g. Chu, 1987, 1989; Avissar and Pielke, 1989; Chen and Avissar, 1994; Avissar, 1995; Pielke, 2001). Such thermally driven local circulations in the convective boundary layer (CBL) are called as the non-classical mesoscale circulations (Segal and Arritt, 1992). Pielke et al. (1991) demonstrate numerically that the mesoscale heat fluxes generated by alternating strips of land and water are usually more significant than turbulent fluxes. The mesoscale heat fluxes are created by various types of landscape discontinuity, and are affected by different background conditions such as wind velocity, thermal stratification, and humidity profiles (Chen and Avissar, 1994). Segal and Arritt (1992) showed that the intensity of the local circulations is critically dependent on the wind speed, as well as the length-scale and amplitude of the surface heat-flux contrast. Dalu et al. (1996) analytically evaluated the vertical heat and momentum fluxes associated with local circulations generated by periodic and isolated surface thermal heterogeneity using a two-dimensional CBL model. They find that for weak or no synoptic wind the vertical velocity is in phase with the diabatic temperature perturbation and for strong synoptic wind the mesoscale perturbation is in the form of the propagation waves that penetrate deeply into the free atmosphere. Landscape variations have their largest influence on generating local circulations for horizontal scales of the order of the Rossby radius (Dalu et al., 1996). The size of the landscape patchiness is an important factor in affecting the CBL structure and generating local circulations (e.g. Avissar and Pielke, 1989).

The local circulation driven by the daytime thermal heterogeneity between oasis and desert may be called the oasis breeze circulation (OBC) with lower branches flowing out of the oasis and upper branches flowing into the oasis and with a downdraft over the oasis. This can be indirectly inferred from the observational results of the downward water vapor flux over the Gobi desert (Wang and Mitsuta, 1992). Vegetation and soil processes and change directly affect the surface energy and moisture fluxes into the atmosphere, and the changes in land-surface properties affect the heat and moisture fluxes within the convective boundary layer (Pielke, 2001).

Sufficient water resources usually maintain the desert oasis. Evident evaporation from the oasis surface cools the oasis. Thus, the oasis is wetter and colder than the surrounding desert that may be called wet–cold island (Su and Hu, 1987) that is confirmed by observational studies using the HEIFE data. The oasis is a wet–cold island inside the desert, especially in the afternoons on fair weather days in June (Kai et al., 1997). An inversion layer over the oasis

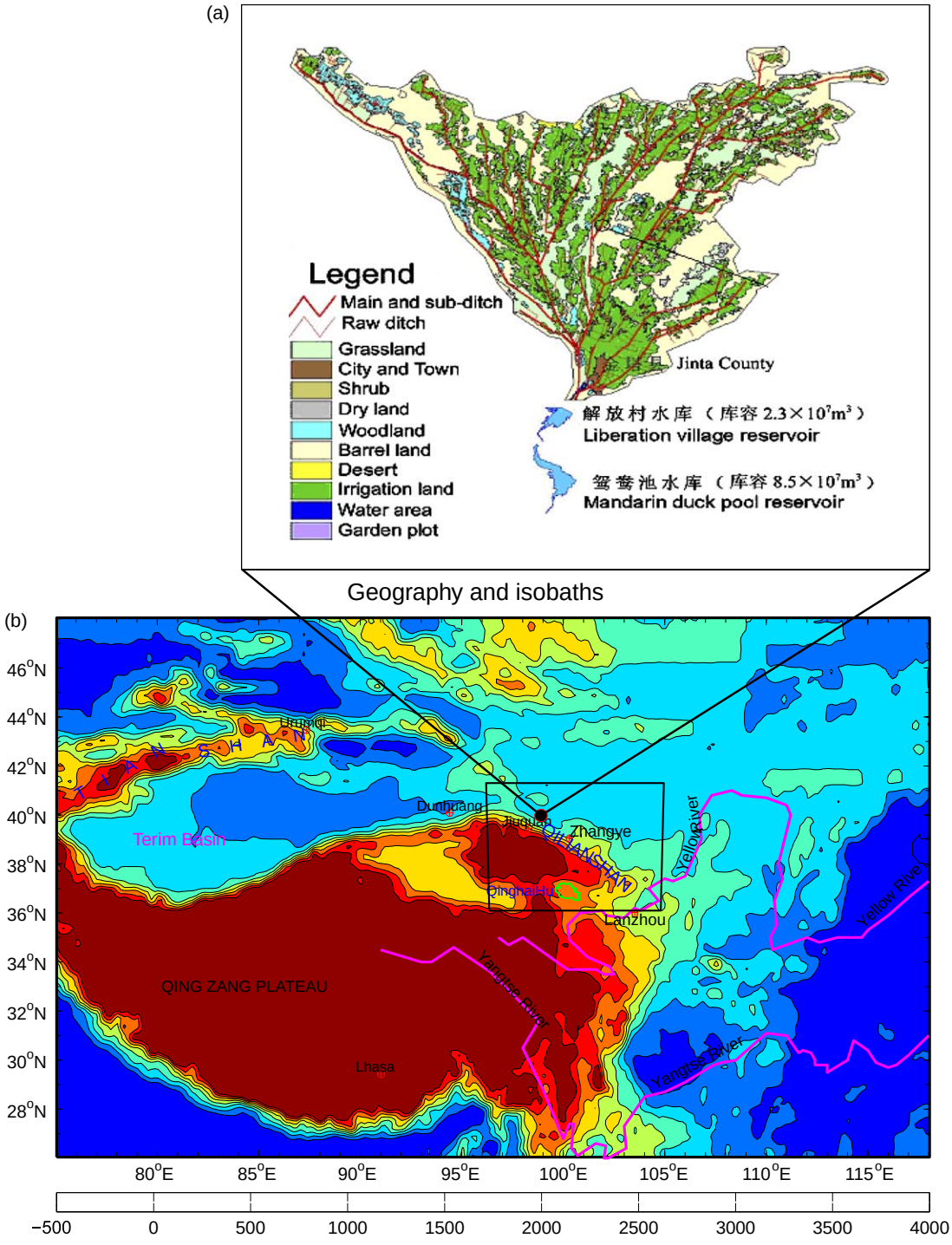

Fig. 1. Oases in northwestern China: (a) Landsat image near Zhangye (horizontal scale around 40 km) showing the geographic features of oases, and (b) topography.

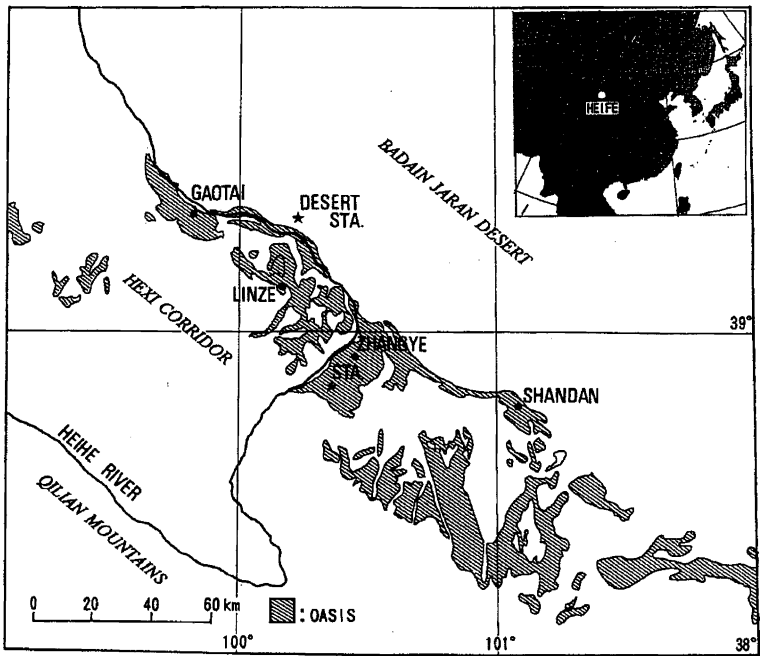

Fig. 2. Map showing the location of the HEIFE experimental site. The oasis regions are shaded (after Kai et al., 1997).

developed from the surface to 8 m height in the afternoon when the wind speed was strong. Between 1 and 8 m heights, the temperature is about 2 °C cooler and the specific humidity is about 2–3 times wetter in the oasis than in the desert (Fig. 3).

With weak or no synoptic wind the oasis patchiness (treated as 'wet and cold islands') may generate OBC that is in phase of the diabatic temperature perturbation. Such a local circulation may protect the oasis from the influence of the surrounding desert in two aspects. The downdraft of the OBC over the oasis may stabilize the atmosphere and in turn reduce the vertical moisture transport (stability mechanism).

2. Surface sensible heat-flux heterogeneity

Temperature over oasis and desert surfaces (T_O, T_D) is determined in such a way that it satisfies the requirement of a surface heat balance. If we assume that the heat capacity of the land-surface is zero, the equations of heat balance requirement over oasis and desert are (Holloway and Manabe, 1971)

$$R^{(O)} = H_S^{(O)} + H_L^{(O)} + G^{(O)},$$
$$R^{(D)} = H_S^{(D)} + H_L^{(D)} + G^{(D)}, \quad (1)$$

where $[R^{(O)}, R^{(D)}]$, $[H_S^{(O)}, H_S^{(D)}]$, $[H_L^{(O)}, H_L^{(D)}]$, and $[G^{(O)}, G^{(D)}]$ are the net radiative flux (downward positive), sensible heat-flux (upward positive), latent heat-flux (upward positive), and soil heat-flux at the oasis and desert, respectively. The difference of the surface energy balance between oasis and desert is represented by

$$R^{(O)} - R^{(D)} = (H_S^{(O)} - H_S^{(D)}) + (H_L^{(O)} - H_L^{(D)}) + (G^{(O)} - G^{(D)}). \quad (2)$$

After analyzing the HEIFE data, Kai et al. (1997) found that the soil flux is almost the same in the oasis and the desert

$$G^{(O)} \approx G^{(D)},$$

which leads to

$$(H_S^{(O)} - H_S^{(D)}) = (R^{(O)} - R^{(D)}) - (H_L^{(O)} - H_L^{(D)}). \quad (3)$$

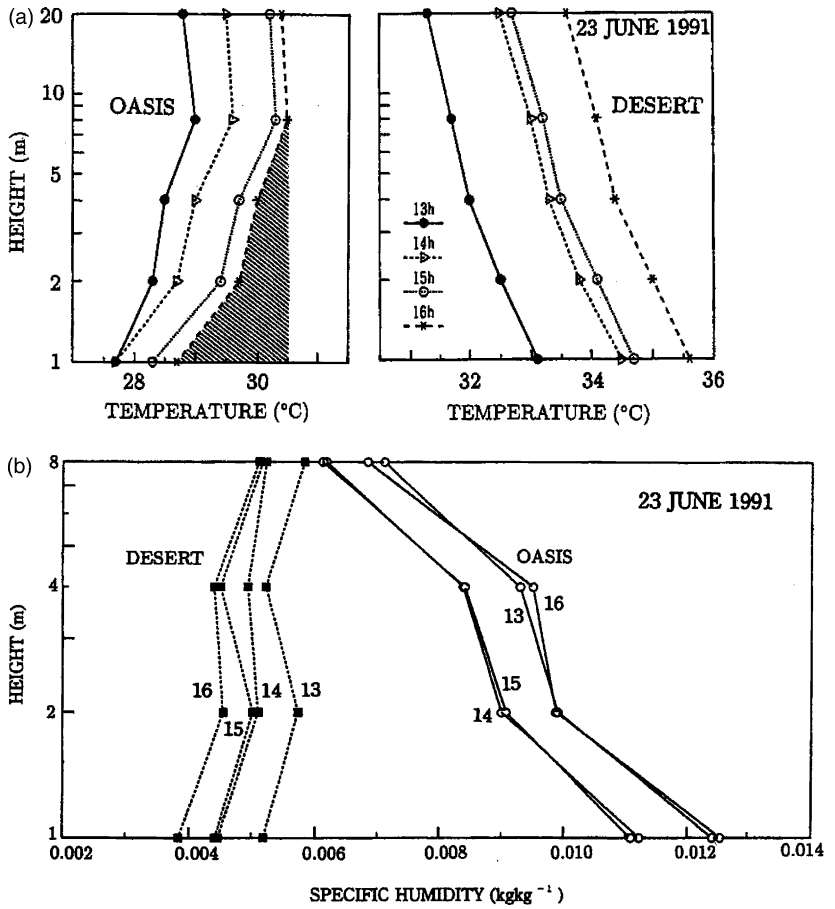

Fig. 3. Observed near surface (a) temperature (°C) and (b) specific humidity profiles in the afternoon of 23 June 1991 during the HEIFE experiment. Note that the local time is marked on the profiles (after Kai et al., 1997).

The characteristics of the surface radiation balance over desert ($R^{(D)}$) and oasis ($R^{(O)}$) are analyzed and compared in the HEIFE area by use of the data observed at the Desert and Zhangye (oasis) stations. Shen et al. (1995) found that under the clear sky, the instantaneous fluxes of downward short- and long-wave radiation reaching the surface and their diurnal variations are nearly the same over desert and oasis. However, due to the surface albedo difference, $R^{(O)}$ is always larger than $R^{(D)}$:

$$R^{(O)} - R^{(D)} \approx 129.6 \text{ W m}^{-2} \quad \text{in summer},$$
$$R^{(O)} - R^{(D)} \approx 16.6 \text{ W m}^{-2} \quad \text{in winter}. \tag{4}$$

Kai et al. (1997) found that the latent heat-flux is an order of magnitudes smaller over the desert (67 W m^{-2}) than over the oasis (634 W m^{-2}) in the HEIFE region

$$(H_L^{(O)} - H_L^{(D)}) \geq 530 \text{ W m}^{-2}. \tag{5}$$

Substitution of (4) and (5) into (3) leads to an estimation fn the difference of the sensible heat-flux between oasis and desert

$$(H_S^{(O)} - H_S^{(D)}) \leq -400 \text{ W m}^{-2}. \tag{6}$$

The differential sensible heat fluxes over the oasis and the surrounding desert regions drive the OBC with the downdraft over the oasis and the updraft over the desert. Surface albedo (larger over the desert than over the oasis) and evaporation (larger over the oasis than the desert) are the two essential and competing factors that determine the sensible heat-flux gradient

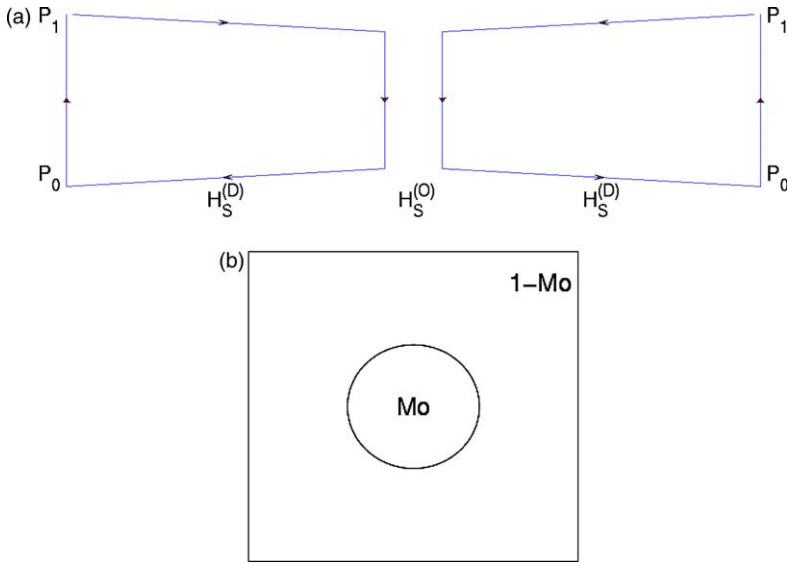

Fig. 4. (a) Oasis breeze circulation driven by sensible heat-flux difference over the oasis and the desert, and (b) illustration of oasis inside the desert. Here, M_o denotes the oasis.

and in turn the OBC (Fig. 4). The albedo effect weakens the OBC and the excessive evaporation from the oasis strengthens the OBC. The horizontal scale for the local circulations such as OBC is on order of the Rossby radius (Dalu et al., 1996).

3. Oasis self-supporting mechanism

Maintenance of the wet–cold island condition leads to the oasis (or the landscape heterogeneity) self-supporting. Large latent heat-flux from the oasis surface leads to excessive heat loss (maintenance of the cold island condition) and water loss (destruction of the wet island condition). Excessive water loss over the oasis surface may eventually destroy the oasis and diminish the landscape heterogeneity.

Strong thermal heterogeneity generates evident local circulations (Avissar and Pielke, 1989; Chen and Avissar, 1994; Avissar, 1995; Dalu et al., 1996). The OBC may decrease the latent heat-flux from the oasis surface through the stability, CBL mechanisms. The low-level hot, dry air over the desert is blocked by the low-level outflow from the oasis and the updraft over the desert. The downdraft of the OBC strengthens the atmospheric stratification that reduces the oasis evaporation (stability mechanism) and causes a shallow cold–wet CBL over the oasis (CBL mechanism).

The oasis self-supporting mechanisms may be enhanced by human activities. Besides the irritation, the tree windbreak is used to preserve the wet–cold island for oasis. For example, Kurose et al. (2002) investigated the wind characteristics and the tree windbreak effect over the oasis in the HEIFE region (Fig. 2) from August 27 to September 12, 1997. The prevailing winds are from west and west to southwest with speed faster than 5 m s^{-1}. The strong (weak) windbreaks are characterized by width larger (smaller) than 1 km, tree arranged at intervals of more (less) than 10 trees/10 m, and tree height longer (shorter) than 10 m. In an oasis with strong windbreaks, the air temperature (T_a) decreased by about 5 °C and the relative humidity increased by 14% compared to the desert outside the oasis.

4. Numerical modeling

The OBC formation and self-supporting mechanisms are simulated using the coupled fifth-generation mesoscale model (MM5) and an advanced land-surface-hydrology model.

4.1. Model description

MM5 is a mesoscale modeling system including advanced model physics was jointly developed by The Pennsylvania State University and National Center for Atmospheric Research (Grell et al., 1994). It is a community mesoscale model widely used for numerical weather prediction, hydrological studies, and air quality studies (Warner et al., 1991; Mass and Kuo, 1998). The non-hydrostatic MM5 Version 3.5 is used in this study.

The land-surface model is coupled to MM5 to describe the effect of vegetation and interactive soil moisture on the surface–atmosphere exchange of momentum, heat, and moisture (Chen and Dudhia, 2001). This LSM is able to provide not only reasonable diurnal variations of surface heat fluxes as surface boundary conditions for coupled models, but also correct seasonal evolutions of soil moisture in the context of a long-term data assimilation system. Also, 1-km resolution vegetation and soil texture maps are introduced in the coupled MM5–LSM system to help identify vegetation/water/soil characteristics at fine scales and capture the feedback of these land-surface forcings. A monthly varying climatological 0.15°× 0.15° green vegetation fraction is utilized to represent the annual control of vegetation on the surface evaporation.

LSM has one canopy layer and the following prognostic variables: soil moisture and temperature in the soil layers, water stored on the canopy, and snow stored on the ground. Four soil layers are used to capture the evolution of soil moisture and to mitigate the possible truncation error in discretization. The thickness of each soil layer from the ground surface to the bottom is 0.1, 0.3, 0.6, and 1.0 m. The precipitation is parameterized by several different schemes. Non-convective precipitation can be represented via an implicit scheme, whereby supersaturated water immediately precipitates, and an explicit scheme including prognostic equations for cloud—water and rainwater. Convective precipitation is parameterized via two cumulus convection schemes. We use the mass flux scheme, which accounts for the effects of penetrative downdrafts (Grell et al., 1994). In the numerical simulation, a flat bottom with elevation of 1460 m is assumed. This indicates that 850 hPa level is nearly at the land-surface. Twenty-three vertical levels are used with 10 hPa at the top of the atmosphere. See the MM5 website http://www.mmm.ucar.edu/mm5/mm5-home.html for more information.

4.2. Triple-nested grid system

A triple-nested grid systems (Fig. 5) with the same center located at 38.9°N, 100.35°E is used in this

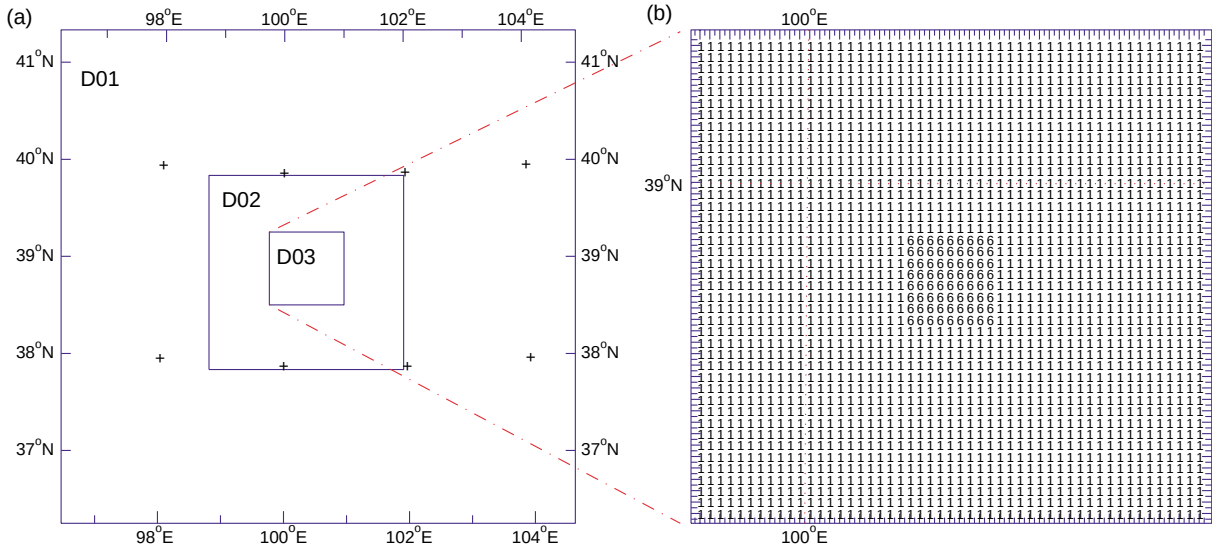

Fig. 5. Illustration of (a) triple-nested grid systems and (b) surface type distribution in the smallest grid system.

study. The first system (large) extends 720 km in the north–south direction and 540 km in the east–west direction with the grid spacing of 9 km. The second system (medium) extends 270 km in the north–south direction and 216 km in the east–west direction with the grid spacing of 3 km. The third system (small) extends 102 km in the north–south direction and 84 km in the east–west direction with the grid spacing of 1 km.

An oasis is located at the center of the third domain. The desert is assumed to be outside of the oasis. Roy and Avissar (2000, GRL) characterized the CBL over domains with meso-gamma-scale (2–20 km) heterogeneity and found two typical length-scales of the processes when the length-scale of the heterogeneity exceeds 5–10 km: (a) 1.5 times the CBL height for turbulent thermals and (b) heterogeneity scale for organized eddies. Three different sizes for oases are used in the numerical experiments to investigate the scale oasis scale effect (Fig. 5): large-oasis (30 km×30 km), medium-oasis (15 km×15 km), and small oases (7.5 km×7.5 km). Only the simulation in the third system (102 km×84 km) is used for the analysis.

4.3. Boundary and initial conditions

At the surface, we use two soil-USGS vegetation types: sand (soil type 1), urban/built-up land for the desert and mixed loam, shrubland/grassland (soil type 6) for the oasis. The cyclic lateral boundary conditions are applied to the first grid system. One way nesting is used for the triple-nested grid system. The larger model provides the lateral boundary conditions for the smaller model using a five point-buffer zone.

The initial condition of the four-layer soil moisture (SM) for the oasis (Table 1) and desert (Table 2) is obtained from recent observations in Zhangye area. The oasis points are initialized as (nearly) saturated soil columns while the desert points are dry. The atmosphere is at rest ($V=0$) with horizontally uniform temperature and specific humidity soundings, which are taken from rawinsonde observation at Zhangye at 00 GMT [0700 LT (LT)] on July 24, 2000 (Fig. 6). MM5–LSM is integrated from the initial conditions with the temporally varying solar irradiance at the top of the atmosphere for the date of July 24, 2002. The time step is 30 s for the first grid system, 10 s for the second grid system, and 10/3 s for the third grid system.

Table 1
Initial conditions of the oasis four-layer soil moistures

Layer	Thickness (m)	Soil moisture (fraction)
1	0.1	0.34
2	0.3	0.33
3	0.6	0.28
4	1.0	0.24

Table 2
Initial conditions of the desert four-layer soil moistures

Layer	Thickness (m)	Soil moisture (fraction)
1	0.1	0.06
2	0.3	0.05
3	0.6	0.04
4	1.0	0.04

5. Wet–cold island

The coupled MM5–LSM model successfully simulates the formation of the wet–cold island over the oasis, generation of OBC, and stabilization of the atmosphere over the oasis. The simulated characteristics for the medium-size oasis (15 km×15 km) are summarized in this section.

5.1. Water storage trend

The total soil moisture over the four layers (surface to 2 m depth)

$$\mathrm{SM}=\frac{h_1\mathrm{SM}_1+h_2\mathrm{SM}_2+h_3\mathrm{SM}_3+h_4\mathrm{SM}_4}{h_1+h_2+h_3+h_4},$$

is simulated by the MM5–LSM model. Temporal evolution of oasis and desert SM indicates stable soil-hydrologic environment (Fig. 7).

5.2. Formation of wet–cold island over the oasis surface

As solar radiation increases during the day (the MM5–LSM model is integrated from 0700 LT),

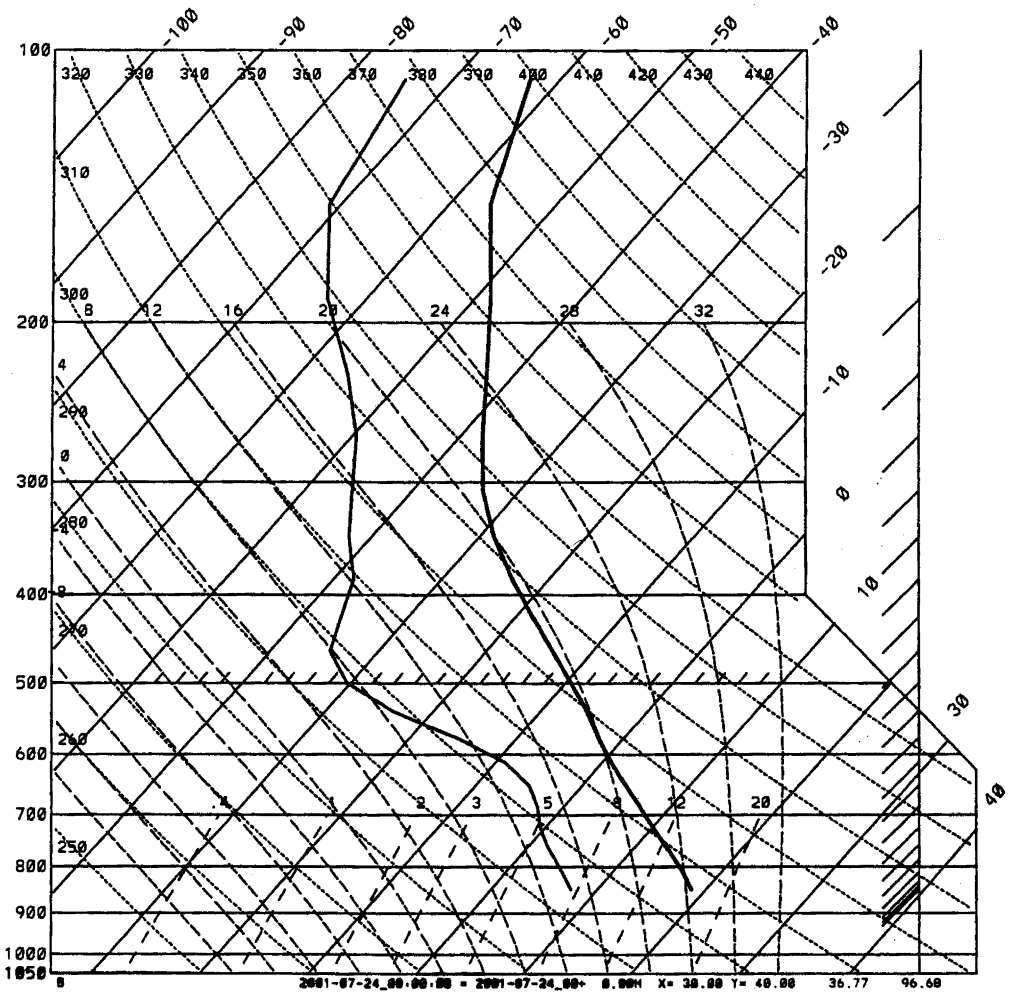

Fig. 6. Observed temperature (thick solid curve) and specific humidity (thin solid curve) soundings at Zhangye at 00 GMT [0700 LT (LT)] on July 24, 2000.

evaporation from oasis surface enhances that makes the oasis surface colder than the surrounding desert surface. At 0600 GMT (1300 LT), a cold (23.5 °C) island forms over the oasis surface (850 hPa) with the surrounding temperature of 25.3 °C over the desert (Fig. 8a) and the cooling effect continues until 1200 GMT (1900 LT, Fig. 8b). The simulated temperature about 2 °C colder over the oasis than over the desert is consistent with the observation (Kai et al., 1997). Although the excessive evaporation from the oasis surface decreases the specific humidity, a high specific humidity zone forms at the vicinity of the oasis at 0600 GMT (1300 LT) with the maximum specific humidity of 7.15 g kg^{-1} (Fig. 9a). At 1200 GMT (1900 LT), a wet island forms over the oasis surface with the maximum specific humidity of 6.54 g kg^{-1}, compared to 5.69–5.99 g kg^{-1} over the desert (Fig. 9b).

The low-level wet–cold island over the oasis surface is caused by the differential surface energy budget between the oasis and the desert. The model simulated surface sensible and latent heat fluxes at 0600 GMT (1300 LT, Fig. 10a) agree well with the observation (Kai et al., 1997): the sensible heat-flux is much smaller in the oasis (68.2 W m^{-2}) than in the surrounding desert (421.0 W m^{-2}); and the latent heat-flux is much larger in the oasis (499.0 W m^{-2})

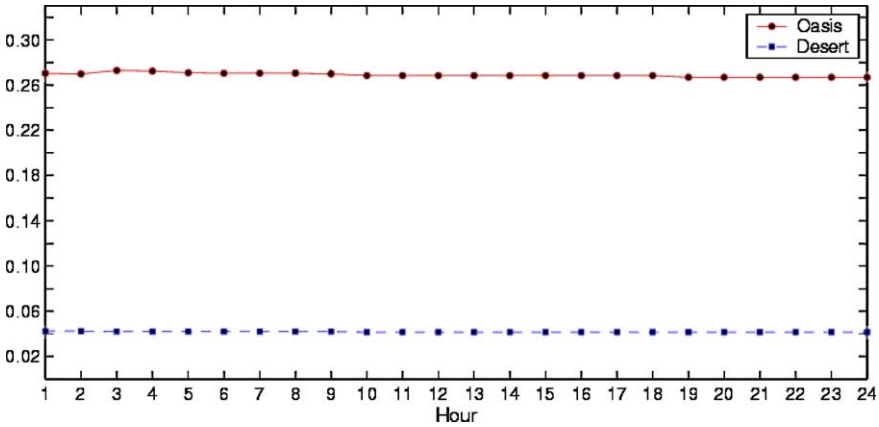

Fig. 7. Simulated temporal variation of total soil moisture (0–2 m) for oasis and desert, showing a stable soil-hydrologic environment.

than in the surrounding desert (110.0 W m^{-2}), as shown in Fig. 11a. The sensible heat-flux difference weakens as the solar radiation reduces. It is still noticeable at 0900 GMT (1600 LT) with 17.7 W m^{-2} at the oasis surface and 26.3 W m^{-2} at the desert surface (Fig. 10b), but not noticeable at 1200 GMT (1900 LT, Fig. 10c). However, the latent heat-flux difference is still strong at 0900 GMT (1600 LT) with 357.0 W m^{-2} at the oasis surface and 80.2 W m^{-2} at the desert surface (Fig. 11b), and at 1200 GMT (1900 LT) with 44.5 W m^{-2} at the oasis surface and 6.1 W m^{-2} at the desert surface (Fig. 11c).

5.3. Low-level divergence and high-level convergence

The model simulates the low-level divergence and high-level convergence pattern and its diurnal variation over the desert oasis. At 0600 GMT (1300 LT), the low-level (850 hPa) winds blow from the oasis to the desert (low-level divergence) with wind speeds above 3 m s^{-1} (Fig. 12a). At 0900 GMT (1600 LT), the wind divergence area slightly increases, but the divergent wind speeds are almost the same as at 0600 GMT (Fig. 12b). At 1200 GMT (1900 LT), the wind divergence area and wind speeds increases drastically. The size of the wind divergence area is around 60 km×60 km, 16 times as large as the oasis. The divergent wind speeds increase to 4 m s^{-1} (Fig. 12c).

At 0600 GMT (1300 LT), the high-level (700 hPa) winds blow from the desert to the oasis (high-level convergence) with wind speeds around 2–3 m s^{-1} (Fig. 13a). At 0900 GMT (1600 LT), the wind convergence area slightly increases, but the convergent wind speeds are almost the same as at 0600 GMT (Fig. 13b). At 1200 GMT (1900 LT), the wind convergence area and wind speeds increases drastically. The convergent wind speeds increase to 4 m s^{-1} (Fig. 13c).

The OBC and its effect on the temperature and humidity are easily identified using the zonal cross-section along 38.9°N (through the center of the oasis). The velocity components (u, w) are plotted associated with temperature (Fig. 14) and specific humidity (Fig. 15). The diurnally varying OBC is simulated with strong downdraft with a maximum value of 38 dPa s^{-1} over the oasis and updraft with a maximum value of 20 dPa s^{-1} over the desert nearly 30 km from the oasis center. The horizontal scale of OBC is around four times as large as the oasis, and the horizontal OBC influence area is around 16 times as large as the oasis.

Low-level (below 700 hPa) downward bending of the temperature contours over the oasis represents the oasis cold-island effect. Such a cold-island effect weakens with altitude (Fig. 14). At 700 hPa, the temperature contours bends a little upward over the oasis, indicating warming there. A high specific humidity ring (enclosed by 6 g kg^{-1} contour) with 10 km width from the surface to 630 hPa level is simulated (Fig. 15) over the desert. The specific humidity is higher in the ring than in the air over the oasis. This high humidity ring encloses the oasis

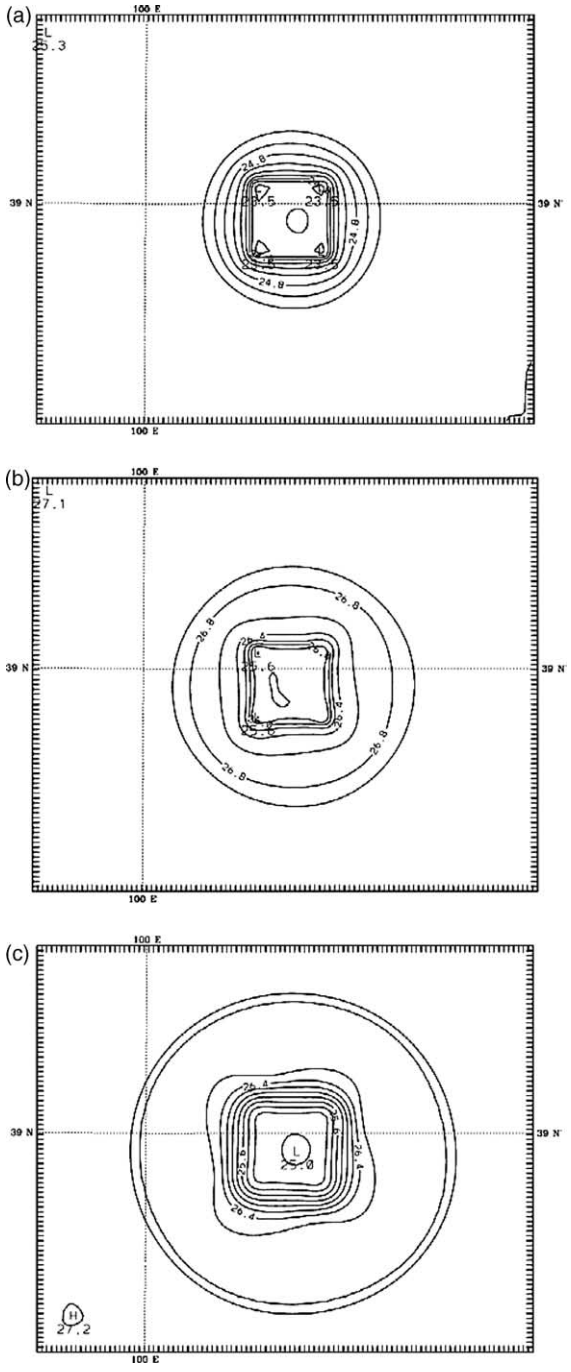

Fig. 8. Simulated surface (850 hPa) temperature (°C) field at (a) 0600 GMT (1300 LT), (b) 0900 GMT (1600 LT), and (c) 1200 GMT (1900 LT).

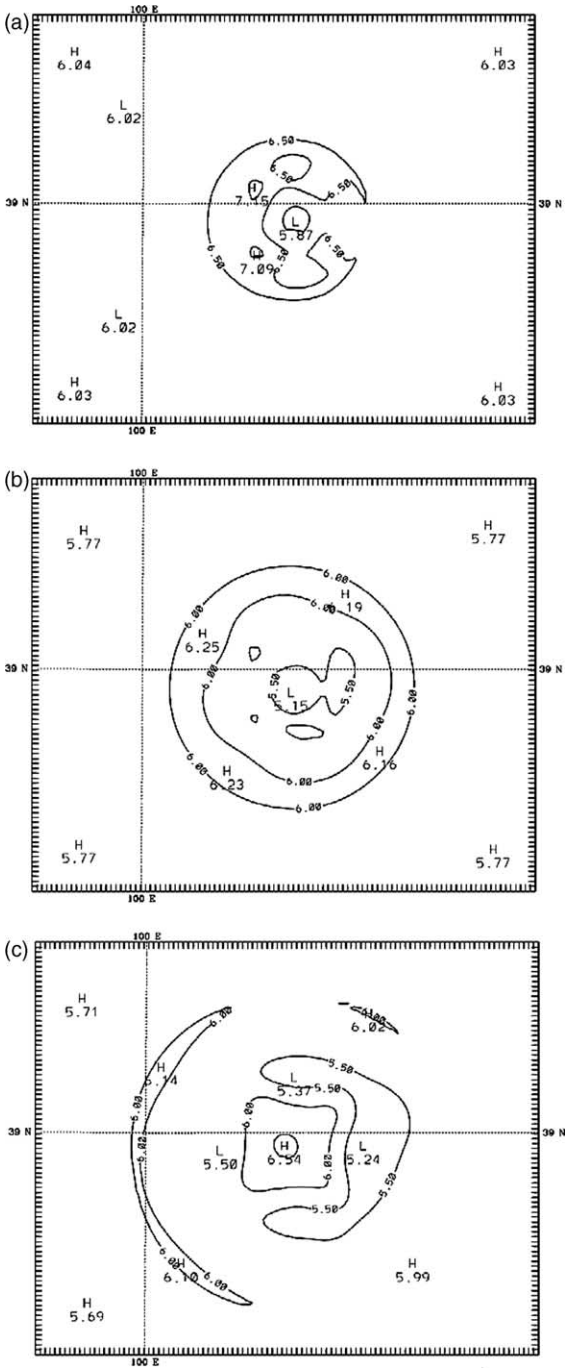

Fig. 9. Simulated surface (850 hPa) specific humidity (g kg^{-1}) field at (a) 0600 GMT (1300 LT), (b) 0900 GMT (1600 LT), and (c) 1200 GMT (1900 LT).

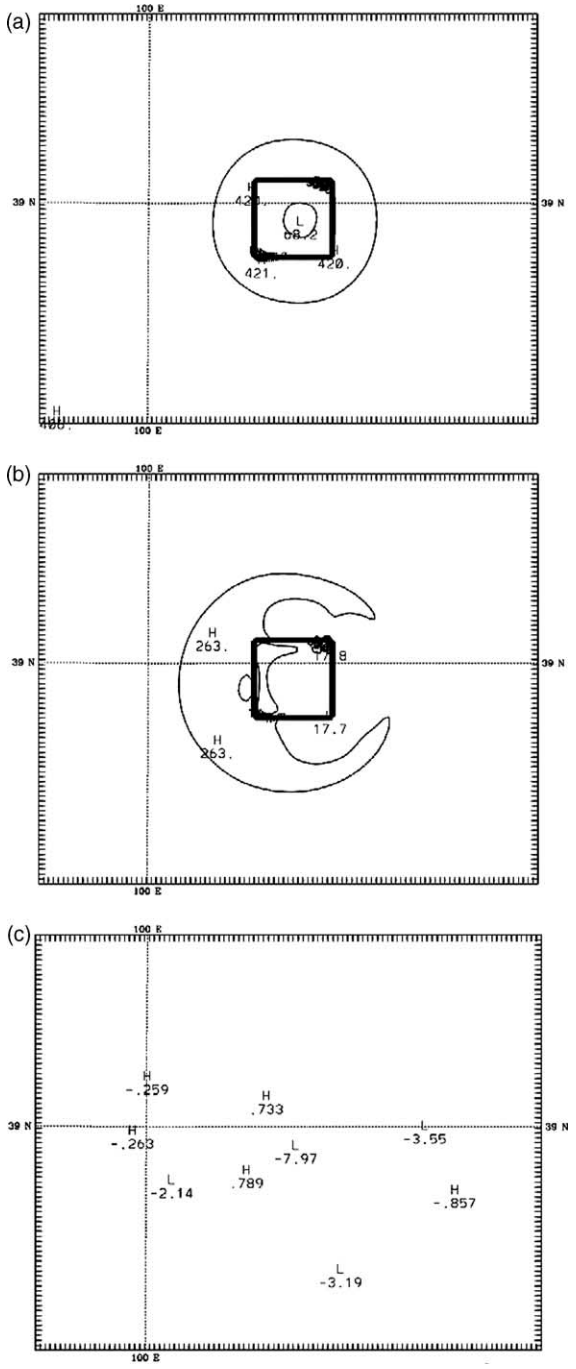

Fig. 10. Simulated surface (850 hPa) sensible heat-flux (W m^{-2}) field at (a) 0600 GMT (1300 LT), (b) 0900 GMT (1600 LT), and (c) 1200 GMT (1900 LT).

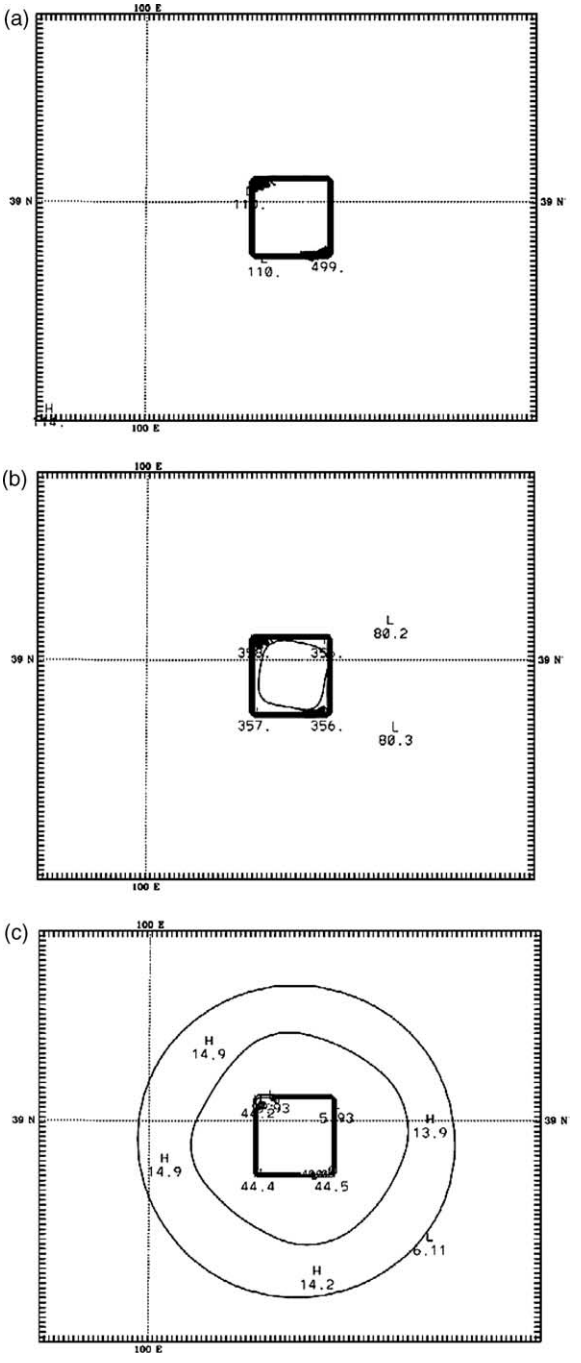

Fig. 11. Simulated surface (850 hPa) latent heat-flux (W m^{-2}) field at (a) 0600 GMT (1300 LT), (b) 0900 GMT (1600 LT), and (c) 1200 GMT (1900 LT).

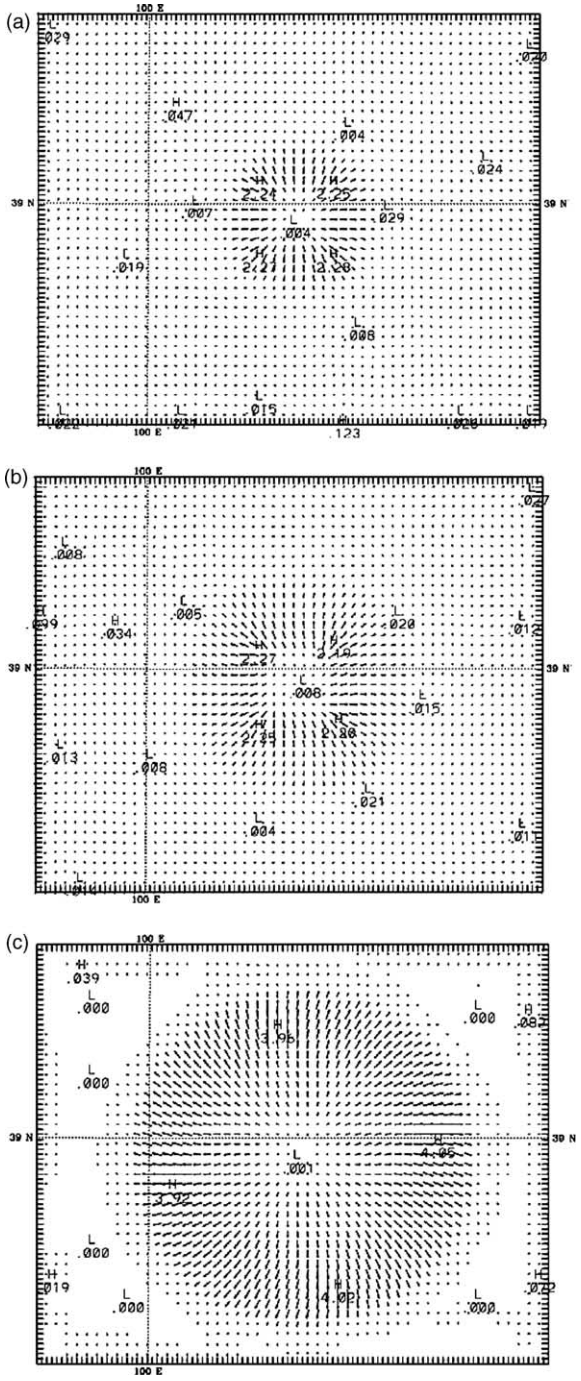

Fig. 12. Simulated surface (850 hPa) wind vector field at (a) 0600 GMT (1300 LT), (b) 0900 GMT (1600 LT), and (c) 1200 GMT (1900 LT).

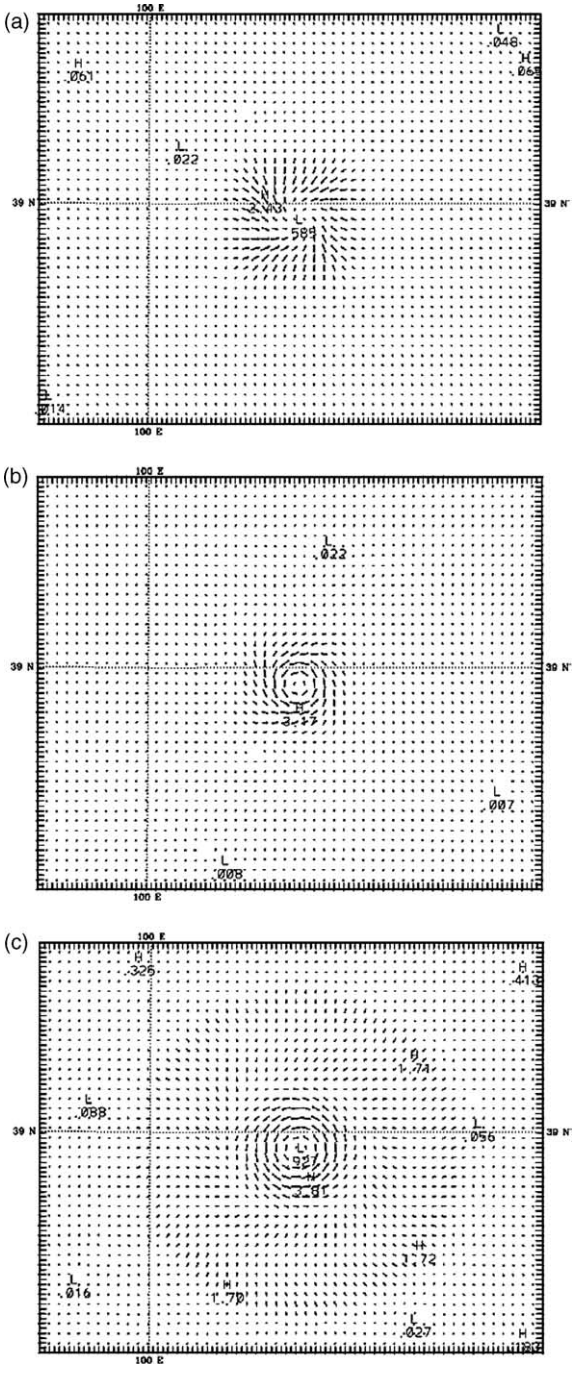

Fig. 13. Simulated upper level (700 hPa) wind vector field at (a) 0600 GMT (1300 LT), (b) 0900 GMT (1600 LT), and (c) 1200 GMT (1900 LT).

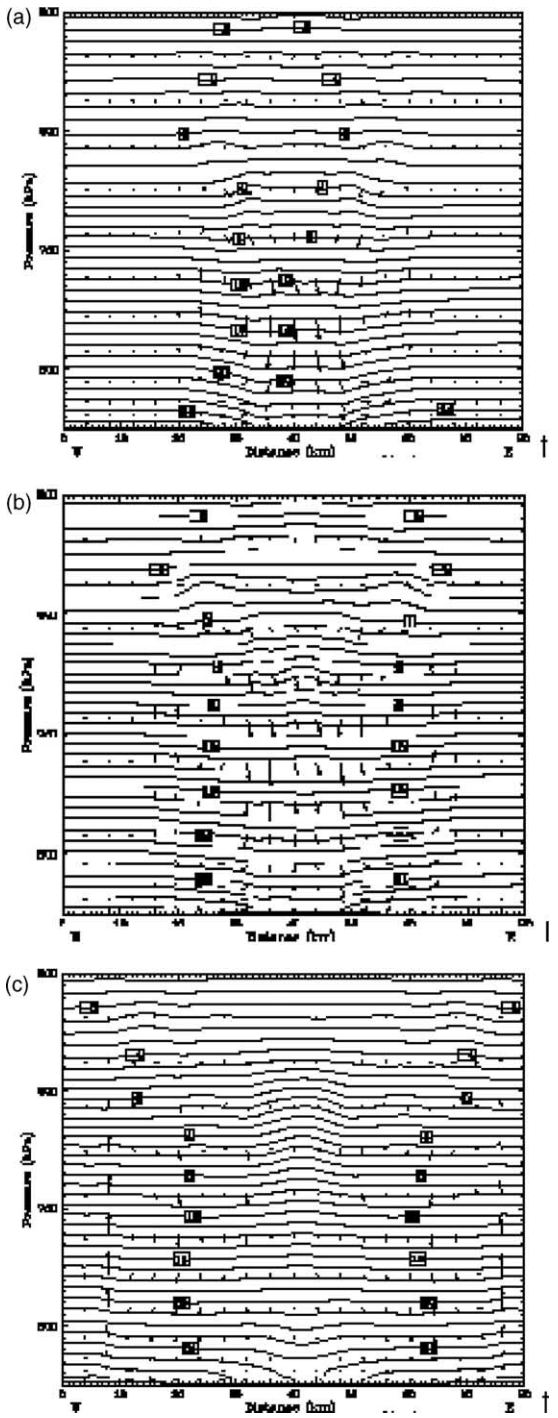

Fig. 14. Simulated zonal cross-sections of temperature (°C) and vertical circulation along 38.9°N at (a) 0600 GMT (1300 LT), (b) 0900 GMT (1600 LT), and (c) 1200 GMT (1900 LT).

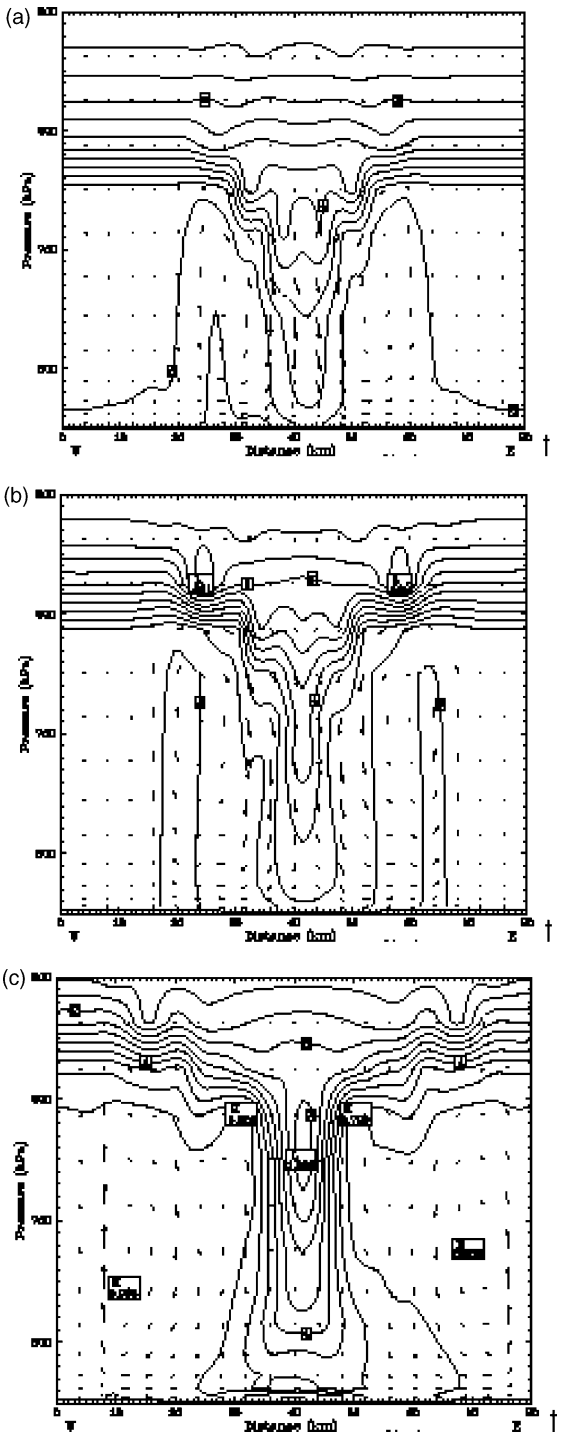

Fig. 15. Simulated zonal cross-sections of specific humidity ($g\,kg^{-1}$) and vertical circulation along 38.9°N at (a) 0600 GMT (1300 LT), (b) 0900 GMT (1600 LT), and (c) 1200 GMT (1900 LT).

and located 20–30 km away from the oasis center. The strong updraft (~ 20 dPa s^{-1}) from the OBC is associated with the high humidity ring all the way from the surface to the top.

5.4. Stability mechanism

The lifted index (LI) is used here to represent the air's stability. It is defined as a rising parcel's temperature when it reaches 500 hPa, subtracted from the actual temperature of the air already at 500 hPa. The larger the LI, the more stable the atmosphere is. A negative LI indicates an unstable atmosphere. The simulated LI fields always have maximum values over the oasis and minimum value over the desert (Fig. 16). For example, LI has a maximum value of 2.05 °C (0.79 °C) over the oasis and a minimum value around −2.00 °C (−3.81 °C) over the desert at 0600 GMT (0900 GMT), as shown in Fig. 15a and b. At early evening, 1200 GMT (1900 LT), LI becomes negative, but its maximum value (−1.02 °C) and minimum value (−5.42 °C) are still over the oasis and desert, respectively (Fig. 16c). The stable atmosphere over the oasis reduces the thermal transfer coefficient and in turn decreases the oasis evaporation rate.

6. Oasis scale effects

The coupled MM5–LSM model is integrated for 24 h with the three oases to investigate the oasis scale effects (Fig. 17): large-oasis (30 km×30 km), medium-oasis (15 km×15 km), and small oases (7.5 km×7.5 km). The numerical simulation for the large-oasis is taken as the control run. For a simulated variable (F), the model differences between the small-oasis (F_s), the medium-oasis (F_m) and the large-oasis (F_l) are represented by

$$\Delta_s F = F_s - F_l, \qquad \Delta_m F = F_m - F_l.$$

In the analysis, the variable F is horizontally averaged over the oases at each time step.

6.1. Wet–cold island

Fig. 18 shows the diurnally varying $\Delta_m T_O$ (solid curve) and $\Delta_s T_O$ (dashed curve), which are positive all

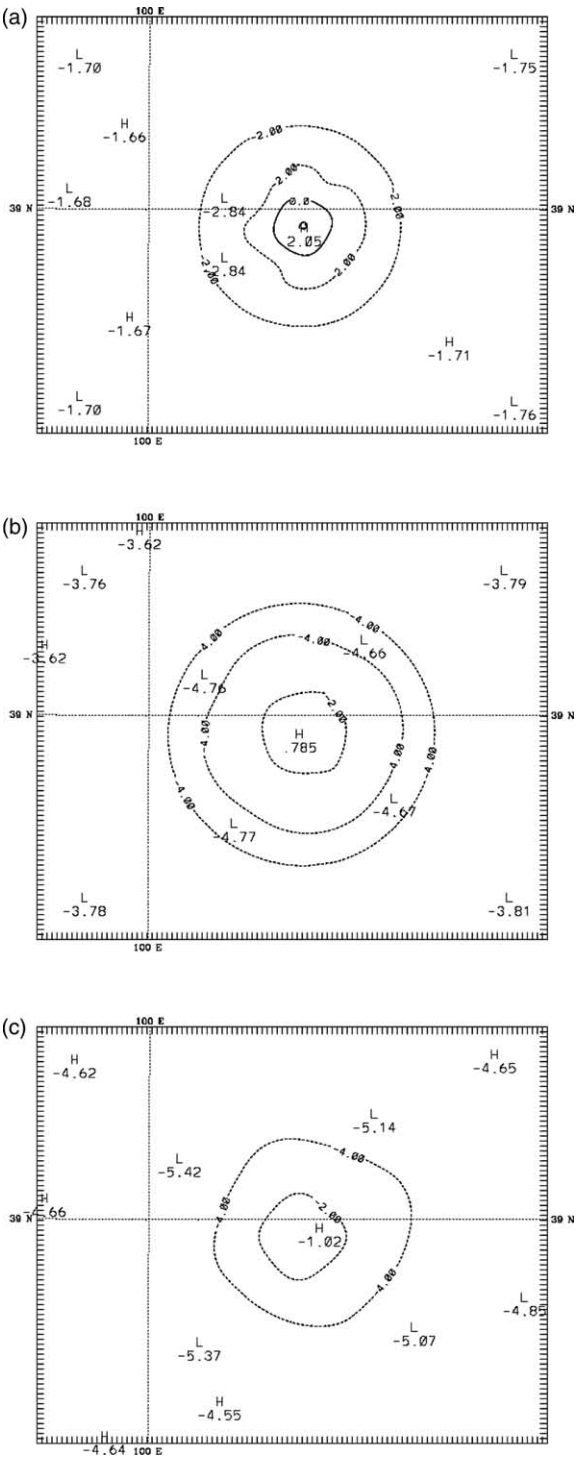

Fig. 16. Simulated lift index (°C) at (a) 0600 GMT (1300 LT), (b) 0900 GMT (1600 LT), and (c) 1200 GMT (1900 LT).

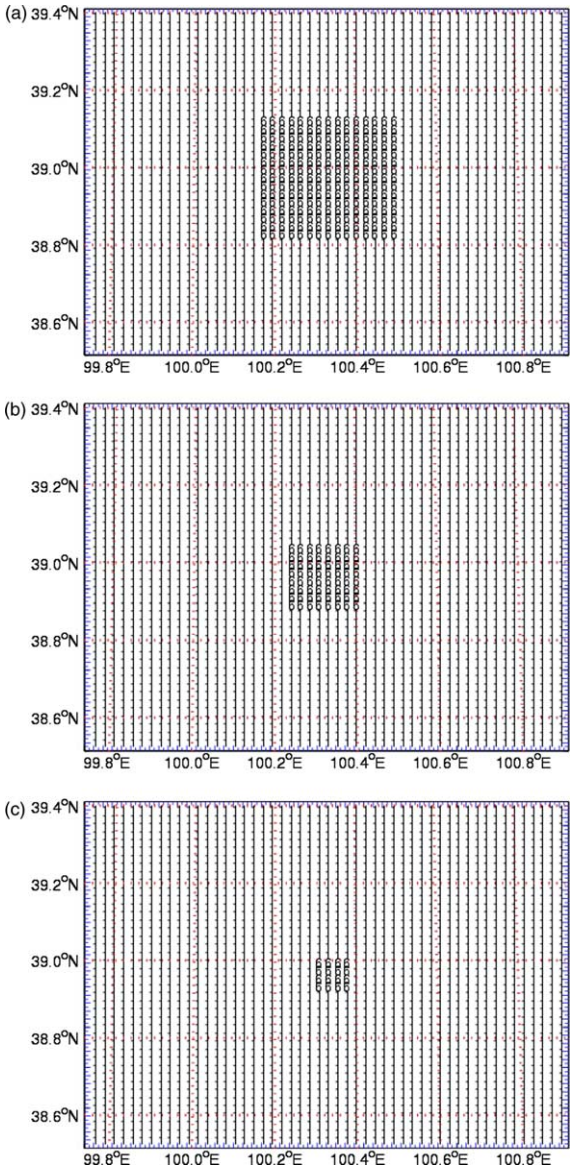

Fig. 17. Three oases in the smallest grid system for numerical investigation: (a) large size with 30 km×30 km, (b) medium size with 15 km×15 km, and (c) small size with 7.5 km×7.5 km. Here, the numbers '6' and '1' denote the oasis and desert, respectively.

the time with maximum values around 0.3 °C for $\Delta_m T_O$ and 0.6 °C for $\Delta_s T_O$ occurring at 1100 GMT (1800 LT). This indicates that the reduction of the oasis size leads to the increase of the oasis surface temperature. Such an increase is more evident at night (1100–2400 GMT) than at daytime (0000–1000

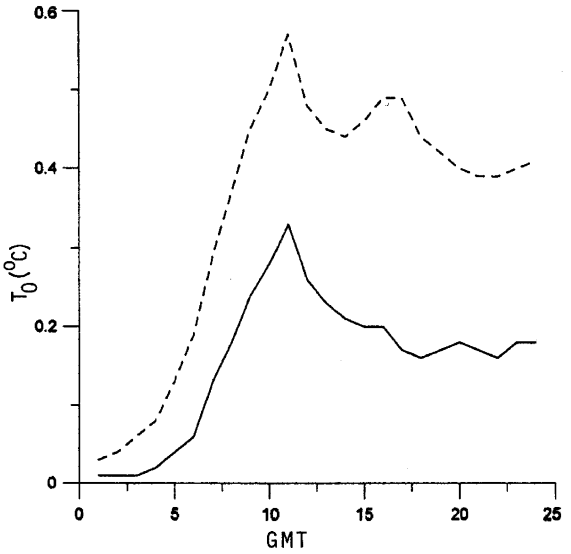

Fig. 18. Subtraction of land-surface temperature (°C) of medium-oasis from large-oasis (solid) and of small-oasis from large-oasis (dashed) simulation.

GMT). At night, $\Delta_m T_O$ varies from 0.3 to 0.2 °C, and $\Delta_s T_O$ changes from 0.6 to 0.4 °C.

Fig. 19 shows the diurnally varying $\Delta_m T_a$ (solid curve) and $\Delta_s T_a$ (dashed curve), which are positive all the time with maximum values around 0.7 °C for

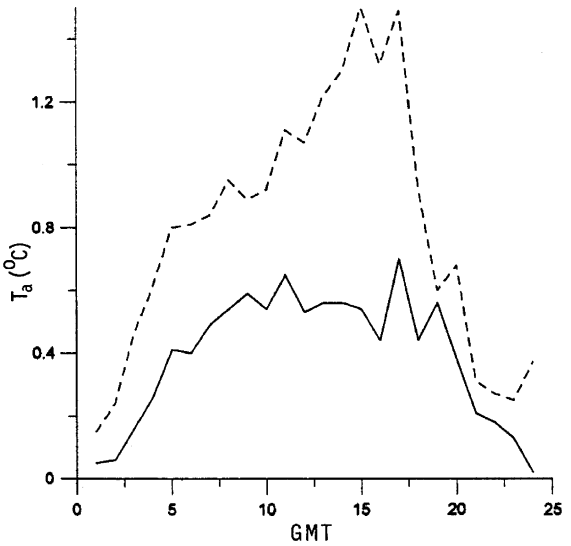

Fig. 19. Subtraction of surface air temperature (°C) of medium-oasis from large-oasis (solid) and of small-oasis from large-oasis (dashed) simulation.

$\Delta_m T_a$ and 1.3 °C for $\Delta_s T_a$ occurring at 1700 GMT (mid-night LT). This indicates that the reduction of the oasis size leads to the increase of the surface air temperature. Such an increase is less evident at 2100–0200 GMT (0400–0900 LT) than the other time. The daily averages of $\Delta_m T_a$ and $\Delta_s T_a$ are around 0.65 and 1.0 °C, respectively. Comparison between Figs. 18 and 19 shows that the oasis scale reduction causes less increase in the oasis surface temperature than in the surface air temperature and in turn reduces the surface sensible heat-flux by reducing the temperature difference ($T_O - T_a$).

Low-level (below 700 hPa) downward bending of the temperature contours over the oasis represents the oasis cold-island effect. Such a cold-island effect weakens when the oasis size reduces (Fig. 20). For the small-oasis, the cold-island effect is not evident (Fig. 20c).

A high specific humidity ring (enclosed by 6 g kg^{-1} contour) over the desert is simulated only for the medium and large oases with 10 km (20–30 km) width from the surface to 630 hPa level for the medium (large) oasis (Fig. 21). The specific humidity is higher in the ring than in the air over the oasis. This high humidity ring encloses the oasis and located 20–30 km away from the oasis center.

6.2. CBL thickness

Calculated CBL thickness is around 3 km over the desert and less than 3 km over the oasis. The CBL thickness is horizontally averaged over the oases at each time step. The horizontally mean PBL thickness (h_{CBL}) has an evident diurnal variation for all the three oases with minimum values at night from 1100 to 2400 GMT (1800–0600 LT). It increases monotonically with time from minimum values at 0000 GMT (0600 LT) to maximum values at 0700 GMT (1400 LT) with 2.3 km for the small-oasis, 1.7 km for the medium-oasis, and 1.3 km for the large-oasis (Fig. 22). The CBL thickness is determined by the atmospheric stability. The more stable the atmosphere, the shallower the PBL thickness is. Thus, the atmosphere is more stable over the large-oasis than over the small-oasis. The daytime oasis self-supporting mechanism due to the atmospheric stability enhances with the oasis size.

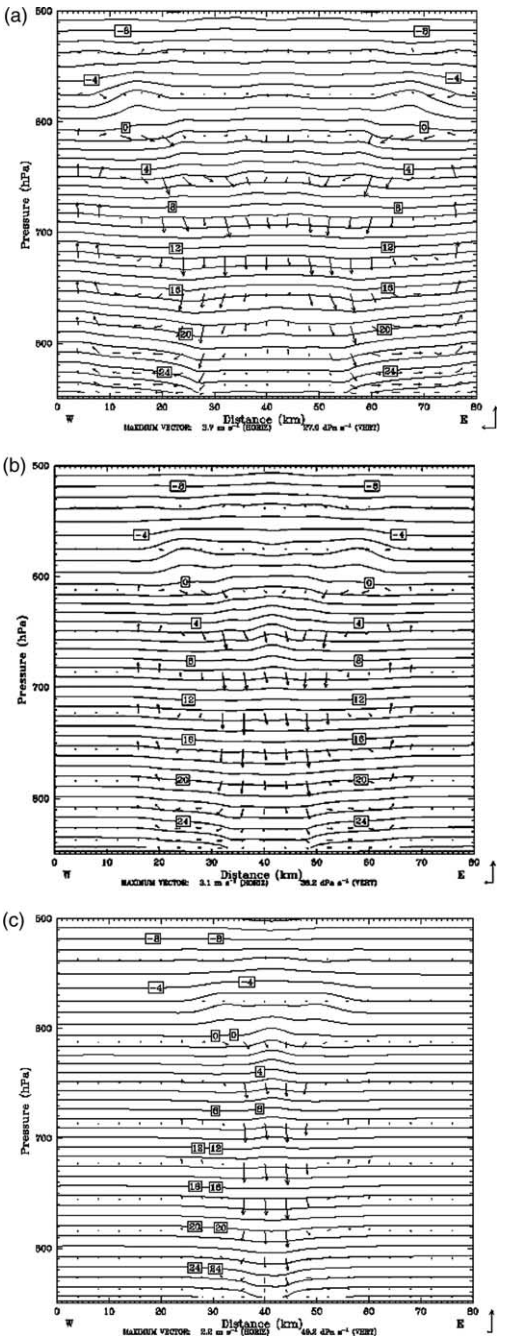

Fig. 20. Simulated zonal cross-sections of temperature (°C) and vertical circulation along 38.9°N at 0900 GMT (1600 LT) for (a) large-oasis, (b) medium-oasis, and (c) small-oasis. In the right lower corner of each panel (from top to bottom), the vertical vectors denote 27.0, 38.2, and 40.2 dPa s^{-1}, and the horizontal vectors denote 3.7, 3.1, and 2.2 m s^{-1}.

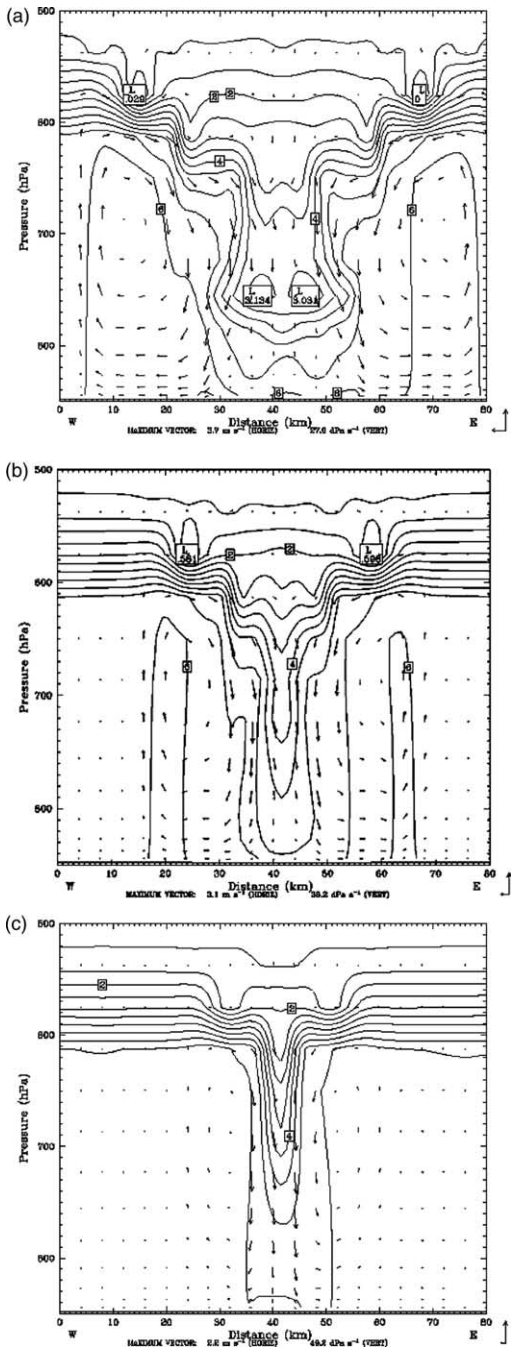

Fig. 21. Simulated zonal cross-sections of specific humidity ($g\,kg^{-1}$) and vertical circulation along 38.9°N at 0900 GMT (1600 LT) for (a) large-oasis, (b) medium-oasis, and (c) small-oasis. In the right lower corner of each panel (from top to bottom), the vertical vectors denote 27.0, 38.2, and 40.2 dPa s^{-1}, and the horizontal vectors denote 3.7, 3.1, and 2.2 m s^{-1}.

6.3. OBC

The zonal cross-section along 38.9°N (through the center of the oasis) is used to represent the OBC and associated temperature and specific humidity. For each oasis, the velocity components (u, w) are plotted associated with temperature (Fig. 20) and specific humidity (Fig. 21). The diurnally varying OBC is simulated for each oasis with a strong downdraft over the oasis and updraft over the desert with different strength depending on the oasis size. The updraft over the desert is evident over the large and medium oases, but not noticeable for the small-oasis. This indicates that the closed vertical circulation occurs only for the large and medium oases. For the large (medium) oasis, the updraft is located over the desert nearly 40 km (30 km) from the oasis center with a maximum value of 20 dPa s^{-1}. The downdraft has comparable strength (maximum value around 38 dPa s^{-1}) among the three oases, but different horizontal length-scales with around 30 km over the large-oasis, 15 km over the medium-oasis, and 7 km over the small-oasis (comparable to the oasis scale). Low-level (below 700 hPa) downward bending of the temperature contours over the oasis represents the oasis cold-island effect. Such a cold-island effect weakens when the oasis size reduces (Fig. 20). For the small-oasis, the cold-island effect is not evident (Fig. 20c).

7. Conclusions

(1) Cooling at the oasis surface and warming at the desert surface drive OBC with downdraft over the oasis and updraft over the desert. Surface cooling/warming is controlled by net surface heat-flux consisting net radiation, sensible heat-flux, and latent heat-flux. Surface albedo (larger over the desert than over the oasis) and evaporation (larger over the oasis than the desert) are the two essential and competing factors that determine the differential surface heating and in turn the OBC. The albedo effect weakens the OBC, and the excessive evaporation from the oasis drives the OBC. The OBC occurrence strongly depends on the oasis scale (i.e. the scale of the thermal heterogeneity). The updraft over the desert is not noticeable for the small-oasis (7.5 km scale), but

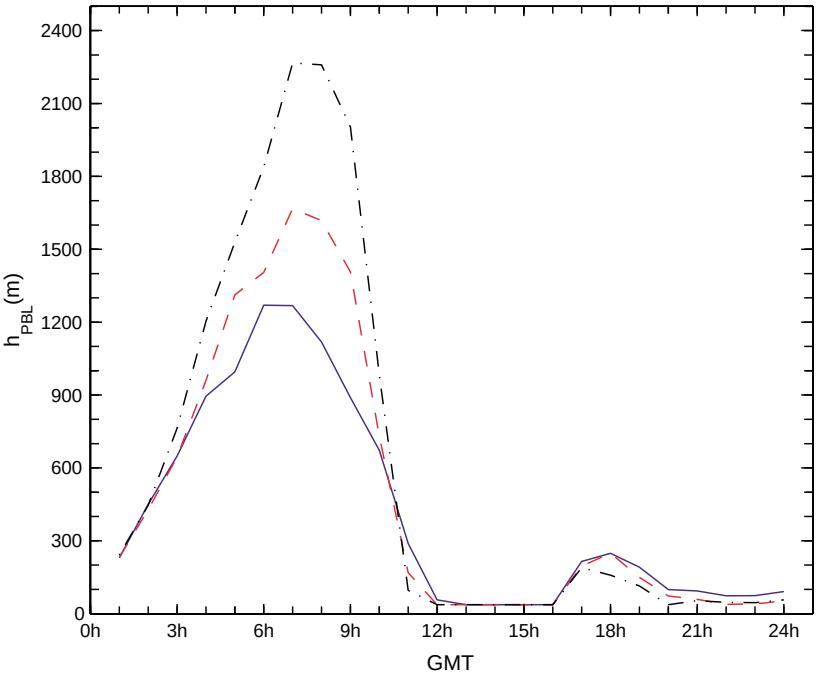

Fig. 22. Simulated planetary boundary layer thickness for large (solid curve), medium (dashed), and small (dotted-dashed) oases.

for the medium-oasis (15 km scale). The OBC and the associated wet ring (oasis self-supporting mechanism) are not simulated for the small-oasis.

(2) The OBC provides a self-supporting mechanism to reduce the heat and moisture exchange between the oasis and the surrounding desert: the downdraft of OBC increases the atmospheric stability that reduces the oasis evaporation (stability mechanism).

(3) Diurnally varying surface sensible and latent heat fluxes and formation of the wet–cold island over the oasis are simulated numerically using the non-hydrostatic MM5 Version 3.5 with a triple-nested grid system and 1 km spacing in the smallest grid system. The model simulated surface heat balance agree well with the observation such that much smaller sensible heat-flux is in the oasis (68.2 W m^{-2}) than in the surrounding desert (421.0 W m^{-2}); and much larger latent heat-flux is in the oasis (499.0 W m^{-2}) than in the surrounding desert (110.0 W m^{-2}) at 0600 GMT (1300 LT).

(4) The simulated OBC is characterized by the low-level wind divergence (850 hPa) and upper-level (700 hPa) wind convergence. The low-level divergence wind speeds increase from 3 m s^{-1} at 0600 GMT (1300 LT) to 4 m s^{-1} at 1200 GMT (1900 LT). The up-level convergence wind speeds increase from 2 to 3 m s^{-1} at 0600 GMT (1300 LT) to 4 m s^{-1} at 1200 GMT (1900 LT). The horizontal length-scale of the OBC is around four times as large as the oasis scale.

(5) The simulated stability mechanism is represented by the maximum values of lifted index over the oasis and minimum values over the desert. The simulated lift index is 2.05 °C (0.79 °C) over the oasis and a minimum value around −2.00 °C (−3.81 °C) over the desert at 0600 GMT (0900 GMT). The stable atmosphere over the oasis reduces the thermal transfer coefficient C_H and in turn decreases the oasis evaporation rate.

(6) As the oasis scale reduces, both oasis surface temperature and surface air temperature increase. However, the increase of the oasis surface temperature is much less than the increase of the surface air temperature. This

causes the reduction of the temperature difference ($T_O - T_a$), and in turn reduces the surface sensible heat-flux. The simulation shows that the sensible heat-flux decreases approximately $10\ W\ m^{-2}$ when the oasis length-scale reduces to half.

(8) As the oasis scale reduces, the surface latent heat-flux usually increases. The maximum increase due to the oasis scale reduction occurs at 0500 GMT (noon LT) with an increase of $10\ W\ m^{-2}$ from the large-oasis (30 km scale) to the medium-oasis (15 km scale) and with an increase of $15\ W\ m^{-2}$ from the large-oasis to the small-oasis (7.5 km scale). This means that the smaller the oasis, the larger the surface latent heat-flux is.

(9) As oasis scale reduces, the PBL thickness increases. At 0700 GMT (1400 LT), the PBL thickness increases from 1.3 km for the large-oasis (30 km scale) to 2.3 km for the small-oasis (7.5 km scale). The PBL thickness indirectly represents the atmospheric stability. The more stable the atmosphere, the shallower the PBL thickness is. Thus, the atmosphere is more stable over the large-oasis than over the small-oasis. The daytime oasis self-supporting mechanism due to the atmospheric stability enhances with the oasis size.

(10) It is noted that large-scale atmospheric motion and topography are neglected in this study. Future studies should include the effects of large-scale motion and topography on the oasis breeze circulation and in turn on the oasis self-supporting mechanism.

Acknowledgements

Peter Chu was supported by the Office of Naval Research, the Naval Oceanographic Office, and the Naval Postgraduate School. Shihua Lu and Yuchun Chen were supported by the Chinese National Science Foundation Key Program 'Observational and Numerical Studies on Oasis Energy and Moisture Budget' (40233035).

References

Avissar, R., 1995. Recent advances in the representation of land–atmosphere interactions in general circulation models. Rev. Geophys. Suppl. 1995;, 1005–1010.

Avissar, R., Pielke, R.A., 1989. A parameterization of heterogeneous land surfaces for atmospheric numerical models and its impact on regional meteorology. Mon. Weather Rev. 117, 2113–2136.

Chen, F., Avissar, R., 1994. The impact of land-surface wetness on mesoscale heat fluxes. J. Appl. Meteorol. 33, 1324–1340.

Chen, F., Dudhia, J., 2001. Coupling an advanced land-surface/hydrology model with the Penn State/NCAR MM5 modeling system. Part I. Model implementation and sensitivity. Mon. Weather Rev. 129, 569–585.

Chu, P.C., 1987. An icebreeze mechanism for an ice divergence–convergence criterion in the marginal ice zone. J. Phys. Oceanogr. 17, 1627–1632.

Chu, P.C., 1989. Relationship between sea surface temperature gradient and thermally forced planetary boundary layer air flow. Pure Appl. Geophys. 130, 31–45.

Dalu, G.A., Pielke, R.A., Baldi, M., Zeng, X., 1996. Heat and momentum fluxes induced by thermal inhomogeneities with and without large-scale flow. J. Atmos. Sci. 53, 3286–3302.

Grell G., Dudhia J., Stauffer D., 1994. A description of the fifth generation Penn State/NCAR Mesoscale Model (MM5). NCAR Technical Note NCRA/TN-398+STR, 117 pp.

Holloway, J.L., Manabe, S., 1971. Simulation of climate by a global general circulation model. Part-1. Hydrologic cycle and heat balance. Mon. Weather Rev. 99, 325–370.

Hu, Y., Gao, Y., Wang, J., Ji, G., Shen, Z., Cheng, L., Chen, J., Li, S., 1994. Some achievements in scientific research during HEIFE. Plateau Meteor. 13, 225–236 (in Chinese with English abstract).

Kai, K., Matsuda, M., Sato, R., 1997. Oasis effect observed at Zhangye Oasis in the Hexi Corridor, China. J. Meteor. Soc. Jpn 75, 1171–1178.

Kurose, Y., Tang, L., Ohba, K., Maruyama, A., Maki, T., 2002. Investigations on some meteorological conditions and evaluation of the effects of tree windbreaks on the improvement of meteorological conditions in Turpan oasis, China. Jpn. Agric. Res. Q. 36, 17–23.

Lin, N.F., Tang, J., Han, F.X., 2001. Eco-environmental problems and effective utilization of water resources in the Kashi Plain, western Terim Basin, China. Hydrol. J. 9, 202–207.

Mass, C.F., Kuo, Y.H., 1998. Regional real-time weather prediction: current status and future potential. Bull. Am. Meteor. Soc. 79, 253–263.

Pielke, R.A., 2001. Influence of the spatial distribution of vegetation and soils on the prediction of cumulus convective rainfall. Rev. Geophys. 39, 151–177.

Pielke, R.A., Dalu, G.A., Snook, J.S., Lee, T.J., Kittel, T.G.F., 1991. Nonlinear influence of mesoscale land-use on weather and climate. J. Climate 4, 1053–1069.

Roy, B., Avissar, R., 2000. Scales of response of the convective boundary layer to land-surface heterogeneity. Geophys. Res. Lett. 27, 533–536.

Segal, M., Arritt, R.W., 1992. Non-classical circulations caused by surface sensible heat-flux gradients. Bull. Am. Meteorol. Soc. 73, 1593–1604.

Shen, Z.B., Tsukamoto, O., Zou, J.L., 1995. The radiative energy budget on the ground surface over desert and oasis in the HEIFE area. J. Meteor. Soc. Jpn 73, 1301–1307.

Su, C., Hu, Y., 1987. Microclimatological characteristics of Hexi Corridor oases and the cold island effect. Chin. J. Atmos. Sci. 11, 390–396 (in Chinese).

Tsukamoto, O., Wang, J., Mitsuta, Y., 1992. A significant evening peak of vapor pressure at an oasis in the semi-arid region. J. Meteor. Soc. Jpn 70, 1155–1159.

Tsukamoto, O., Sahashi, K., Wang, J., 1995. Heat budget and evapotranspiration at an oasis surface surrounded by desert. J. Meteor. Soc. Jpn 73, 925–935.

Wang, J.M., Mitsuta, Y., 1992. An observational study of turbulent structure and transfer characteristics in Heihe oasis. J. Meteor. Soc. Jpn 70, 1147–1154.

Warner, T.T., Kibler, D.F., Steinhart, R.L., 1991. Separate and coupled testing of meteorological and hydrological forecast models for the Susquehanna River Basin in Pennsylvania. J. Appl. Meteor. 30, 1521–1533.